Available online at www.sciencedirect.com
ScienceDirect
Optics Communications 280 (2007) 271–277
OPTICS COMMUNICATIONS
www.elsevier.com/locate/optcom

Experimental demonstration and cascadability analysis of a tunable optical buffer based on a re-circulating loop consisting of optical SSB modulator and FBG filter

Xinyu Xu [a], Yikai Su [a,*], Lufeng Leng [b]

[a] State Key Lab of Advanced Optical Communication Systems and Networks, Shanghai Jiao Tong University, Shanghai 200240, China
[b] New York City College of Technology, City University of New York, Brooklyn, NY 11201, USA

Received 9 February 2007; received in revised form 6 July 2007; accepted 9 August 2007

Abstract

We demonstrate a tunable optical buffer with variable time delays for label switching applications using an optical single sideband modulator in a fiber Bragg grating-filter loop. This optical buffer realizes payload storage with optional wavelength conversion function, providing flexibility in packet router design. Small sensitivity penalty is observed in our experiment after the payload circulating in the buffer loop three times. The cascadability of the tunable optical buffer is investigated. We provide analysis of the optical signal to noise ratio degradation due to accumulated amplified spontaneous emission noise, and the penalty caused by loss ripple and group delay ripple of the fiber Bragg grating.

Keywords: Optical label switching (OLS); Optical single-sideband (SSB) modulator; Optical buffer; Wavelength conversion; Fiber Bragg grating (FBG); Group delay ripple (GDR); Loss ripple (LR)

1. Introduction

As a key component in optical label switching (OLS) [1,2] implementations, optical buffer has attracted considerable attentions. Several techniques have been proposed and demonstrated to realize optical buffers, such as fiber delay line (FDL) [3–5], slow lights [6,7], folded-path time delay [8,9] and frequency conversion loops [10,11]. Among them, FDL based buffer is a common solution to optical signal contention for its ability to achieve various time delays, but the buffer size becomes physically large with increasing number of storage stages. In addition, the requirements on precision control make it less flexible. With fine tuning capability, slow-light based buffers can normally achieve small amount of delay of several bits, which, however, is not sufficient for practical applications. The folded-path buffers can also achieve variable time delays, however, it becomes complex to control many on-off reflectors in each stage as the number of delay-line segments increases. Besides these schemes, wavelength-conversion-loop based optical buffer is an interesting method due to its small size and flexible adjustment of the time delay, which was varied by changing the frequency shift [10,11]. However, the wavelength of the output signal through the buffer was inevitably shifted from that of the input signal, which is not always desirable in packet routers.

In this paper, we demonstrate a tunable optical buffer for label switching, which can achieve variable time delays with or without wavelength change, thus facilitating flexible router designs. We also study the cascadability of such a buffer, which was not addressed before. The buffer is configured as a wavelength-selective circulating loop mainly consisting of an optical single sideband (SSB) modulator, an optical circulator, and a fiber Bragg grating (FBG).

* Corresponding author. Tel.: +86 021 34204356; fax: +86 021 34204370.
E-mail address: yikaisu@sjtu.edu.cn (Y. Su).

0030-4018/$ - see front matter © 2007 Elsevier B.V. All rights reserved.
doi:10.1016/j.optcom.2007.08.026

The wavelength up and down conversions can be controlled by properly adjusting the bias of the SSB modulator. Label separation and payload storage based on such a tunable buffer are experimentally demonstrated. Analysis of the buffer cascadability performance is also presented, and optical signal to noise ratio (OSNR) penalty due to amplified spontaneous emission (ASE) noise accumulation is studied. We also investigate the combined effects due to loss ripple (LR) and group delay ripple (GDR) of the fiber Bragg grating(FBG), which had not been considered before our work.

2. Principle of operation

The structure of the optical buffer for optical label switching is shown in Fig. 1. The CW lights from two separate laser diodes (LDs) at different wavelengths are modulated by two Mach-Zehnder modulators (MZMs) to generate the label and the payload signals, respectively. An optical coupler (OC) following the MZMs combines the label and the payload to form the packets. At an intermediate node, the label is separated through the reflection port of FBG1 [12,13], and then sent to an optical-to-electrical (O/E) converter before being fed into a bit error ratio tester (BERT) for label detection. In the meantime the payload passes through FBG1 as its wavelength is outside the reflection bandwidth of FBG1, and then enters the optical buffer. In the buffer loop, an erbium doped fiber amplifier (EDFA) compensates the loss of the loop, and a bandpass filter (BPF) reject the out-of-band noise accumulated in the loop. The DC bias control of the optical SSB modulator determines the relative phase difference between the two parallel MZMs inside the SSB modulator [14], thus enabling up or down wavelength shift of the payload. The wavelength shift interval is determined by the frequency of the RF driving signal applied on the SSB modulator. The time delay of a circulation in the loop is the sum of the propagation times through the EDFA, the filter, the optical SSB modulator, the circulator, and the fibers.

Here we discuss the buffer operation in detail. Suppose the center wavelength of the input payload is λ_0, which is initially outside the reflection band of FBG2, and there is no overlap between the payload spectrum and the bandwidth edge of the grating, as shown in Fig. 2a. When the payload enters the optical buffer loop for the first time, its wavelength is not shifted until it reaches the SSB modulator, where the voltage of the programmable bias is fixed at a high level to shift the wavelength down by $\Delta\lambda$ as shown in Fig. 2b. Here the choice of $\Delta\lambda$ is determined by the bandwidth of the payload signal and the edge slope of FBG2, and $\Delta\lambda$ should be large enough to avoid overlap between the spectrum of the payload and the edge of FBG2. After passing through the SSB modulator, the center wavelength of payload becomes $\lambda_0 - \Delta\lambda$, which is within the reflection bandwidth of the grating. Therefore, the payload is almost totally reflected by the high reflectivity grating and fed back to the input of the buffer through a polarization controller (PC). The wavelength of the payload can be shifted to a higher or lower one by properly switching the applied voltage at the DC bias of the modulator in the corresponding time slot, so that the payload can re-circulate in the loop as long as needed. Once the wavelength of the payload is shifted outside the reflection bandwidth of the grating, the payload will exit the optical buffer. Here the wavelength of the output payload may maintain its original value, or down-shifted by a multiple of $\Delta\lambda$ to appear outside the lower edge of the reflection bandwidth. The achievable number of circulations of the payload in the buffer can be large as long as the shifted wavelength resides within FGB2's reflection bandwidth and the signal quality does not degrade significantly.

Fig. 2 illustrates a 3-loop circulation of the payload without wavelength change at the exit. The payload with 3-loop circulations experiences wavelength shifts in the sequence of $\lambda_0 \rightarrow (\lambda_0 - \Delta\lambda) \rightarrow (\lambda_0 - 2\Delta\lambda) \rightarrow (\lambda_0 - \Delta\lambda) \rightarrow \lambda_0$. The DC bias of the SSB modulator is fixed at high voltage while the payload circulates twice and its wavelength is shifted to $\lambda_0 - 2\Delta\lambda$, which is still within the reflection bandwidth of FBG2. Then the DC bias of the SSB modulator is switched to low voltage so that the wavelength can be shifted back to λ_0 after the payload traverses the modulator twice, as shown in Fig. 2b. Finally the payload passes through FBG2 and exits the buffer without wavelength change. The timing control of the buffer loop operation is achieved through the use of a gate voltage generator, which provides the voltage signal for the DC bias of the SSB modulator for frequency up/down conversion. In addition, if wavelength change is desired, the DC bias

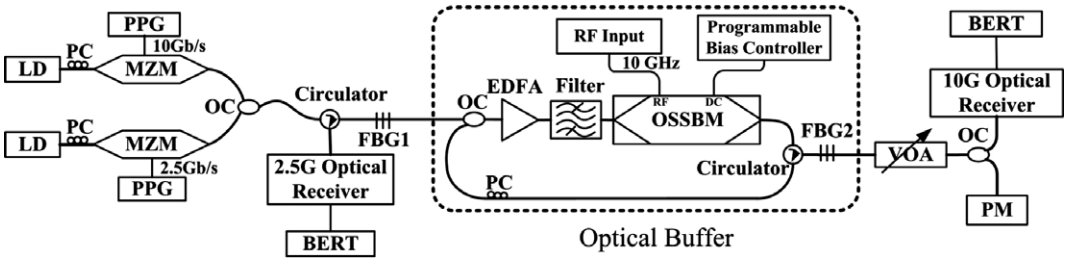

Fig. 1. Experimental schematic. LD: Laser Diode, MZM: Mach-Zehnder Modulator, PPG: Pulse Pattern Generator, PC: Polarization Controller, OC: Optical Coupler, FBG: Fiber Bragg Grating, EDFA: Erbium-doped Fiber Amplifier, VOA: Variable Optical Attenuator, OSSBM: Optical Single-Sideband Modulator, BERT: Bit Error Ratio Tester, PM: Power Meter.

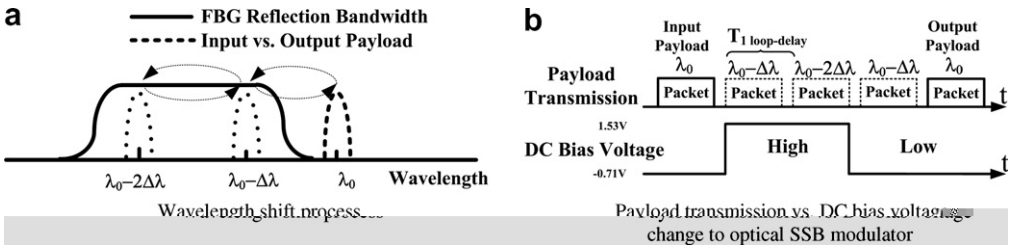

Fig. 2. 3-loop circulation of the payload. (a) Wavelength shift process (b) Payload transmission vs. DC bias voltage change to optical SSB modulator.

can be kept high throughout the circulations so that the wavelength of the payload repeatedly shifts towards the lower wavelength until it is outside the reflection bandwidth of FBG2.

3. Experimental results

In this experiment, the central wavelengths of the label and the payload are 1549.41 nm and 1549.56 nm, respectively. Both the label and the payload are encoded in non-return-to-zero (NRZ) format. The label is a 2.5 Gb/s pseudo-random bit sequence (PRBS) with 2^{23}-1 bit length. For the payload generation, the pulse pattern generator (PPG) is set to zero substitute mode so that a 2767 bit pattern can be obtained from a 2^{15}-1 PRBS at 10 Gb/s. The time delay of the buffer corresponds to the payload length. In our experiment, the bit length of the payload is 2^{15}-1 PRBS at 10 Gb/s, thus the delay equals ~320 ns. The power of the payload is −3.25 dBm when it is launched into the optical buffer. The RF driving signal for the optical SSB modulator is a 10 GHz sine wave, which is the clock generated by the same PPG. The central wavelength of FBG2 is 1549.42 nm with a 0.178 nm reflection bandwidth, As shown in Fig. 3a. The characteristic of FBG1 is similar to that of FBG2 with the same central wavelength and slightly narrower reflection bandwidth, which is not shown. The reflectivity of FBG2 is nearly 95%. Fig. 3 shows the optical spectrum of the payload with various time delays: 1-loop delay, 2-loop delay, and 3-loop delay. The payload with 2-loop circulations undergoes 1549.56 nm → 1549.48 nm → 1549.40 nm → 1549.32 nm, with 1549.32 nm being outside the reflection bandwidth of FBG2. Here the wavelength shift interval is $\Delta\lambda = 0.08$ nm, corresponding to 10 GHz frequency shift. The difference between the payload spectra in Fig. 3a and b is mainly due to the degradation of the SSB modulation and the power leakage through the transmission port of FBG2, which is induced by the imperfect reflectivity of the grating. In Fig. 4 we show the output payload after FBG2 with various time delays in the time domain, and the corresponding electrical waveforms at the 10G optical receiver output are also provided. The time delay of one circulation is about 320 ns. Fig. 4a provides the waveform of the back-to-back payload signal without delay. Fig. 4b shows the output payload after one circulation without wavelength change. Due to insufficient isolation between the transmission and the reflection ports of FBG2, residual powers are observed in the optical domain at the transmission port of FBG2, however this signal leakage can be reduced if a FBG with higher reflectivity is employed. These residual powers are suppressed in the electrical domain by tuning the detection threshold of the 10G optical receiver. By properly adjusting the DC bias of the SSB modulator, the payload can circulate twice with wavelength conversion (Fig. 4e) and three times without wavelength change (Fig. 4f). The corresponding optical spectrum of the payload is provided in Fig. 3b. Limited by the programming capability of the bias controller in this experiment, we demonstrated up to 3-loop payload circulation.

For the BER measurements, the BERT was set in 'zero substitue' mode. Therefore, gating was not required. BER measurements versus the received powers for the label

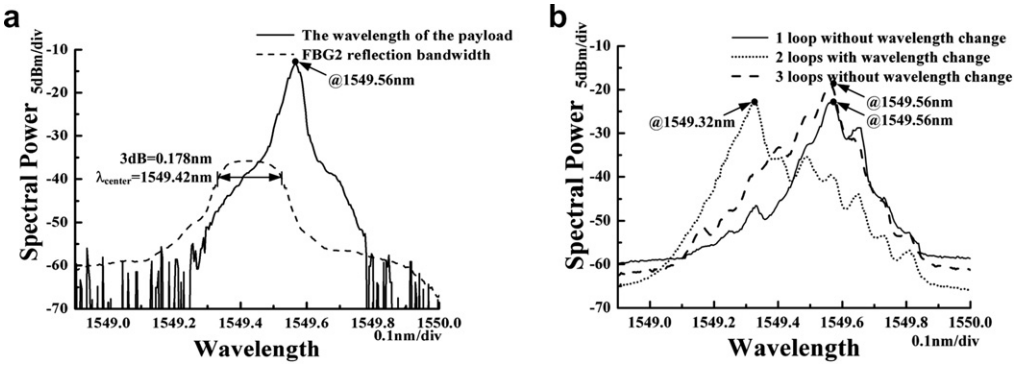

Fig. 3. Optical spectra (a). The FBG reflection bandwidth and the wavelength of the payload (b). Optical spectra of the output payload with various time delays.

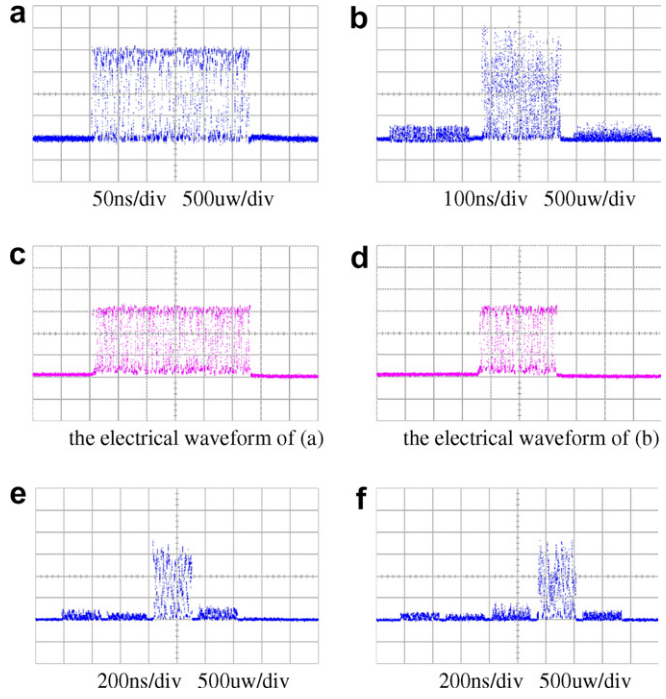

Fig. 4. The payload waveforms with various time delays in the optical domain, and the corresponding electrically detected waveforms after(a) the Mach-Zehnder modulator, (b) one circulation without wavelength conversion, (e) two circulations with wavelength conversion, (f) three circulations without wavelength conversion.

and the payload are provided in Fig. 5, respectively. As the label is detected by a high-sensitivity APD receiver while the payload detection employs a conventional PIN receiver, the receiver sensitivities for the label and the payload are different; on the other hand, different bit rates also lead to different receiver sensitivities. Fig. 5a shows the BER curves for the label under the back-to-back condition and after separation from the packet, and the power penalty is less than 1 dB. Fig. 5b provides the BER curves for various numbers of circulations, and ~0.5 dB power penalty is observed after the payload circulates three times in the buffer. Due to certain drifting of the FBG2 that causes the non-uniform filtering for signals, the payloads with 2-loop and 3-loop circulation suffer more filtering effects than the payload with 1-loop circulation. Therefore, the penalty gap is non-linear.

4. Cascadability analysis and simulation results

Cascadability is important in evaluating the optical buffer performance. In our analysis, circulation of signals in the buffer can be considered as through cascaded segments, with each segment consisting of the EDFA, the filter, the optical SSB modulator, the circulator, the FBG2, and the fibers. The ASE noise accumulation could be a major factor limiting the buffer performance [15]. In addition, the loss ripple (LR) and group delay ripple (GDR) [16,17] of the FBG2 are common imperfections inducing OSNR penalties in the buffer.

We study the impact of the ASE noise accumulation in cascaded amplifier systems [18]. The output OSNR is written as:

$$\mathrm{OSNR_{dB}} = 58 + P_{\mathrm{in}} - \mathrm{NF} - 10\lg(N) \quad (1)$$

where P_{in} is the input signal power into the optical buffer, NF is the noise figure of the amplifier, and N is the number of signal circulations in the buffer. The calculated OSNR versus the number of signal circulations (N) is presented in Fig. 6.

In Eq. (1) the effects of LR and GDR of the filters are ignored, however they are common factors inducing signal power loss and OSNR degradation as discussed in [16,17], where Liu et al. studied the OSNR penalty of a signal through the passband of an optical component. The penalty caused by the combined LR and GDR effects, though, has not been addressed before. Here we investigate the OSNR penalty induced by the combined LR and GDR effects through analytical study and numerical simulations. In practice, the OSNR penalty is related to the eye opening penalty (EOP) of the received signal [19] in the low BER regime, while the EOP can be calculated from the eye diagram distortion induced by the LR and GDR effects through transmission in the optical buffer. The transfer function of the FBG after the i-th circulation can be defined as:

$$T_i(f) = L_i(f)^* e^{jG_i(f)} \quad (2)$$

where $L_i(f)$ and $G_i(f)$ are the transfer functions of LR and GDR of the FBG, respectively, and f is the frequency in the bandwidth of the FBG. $L_i(f)$ can be generally expressed in decibels as:

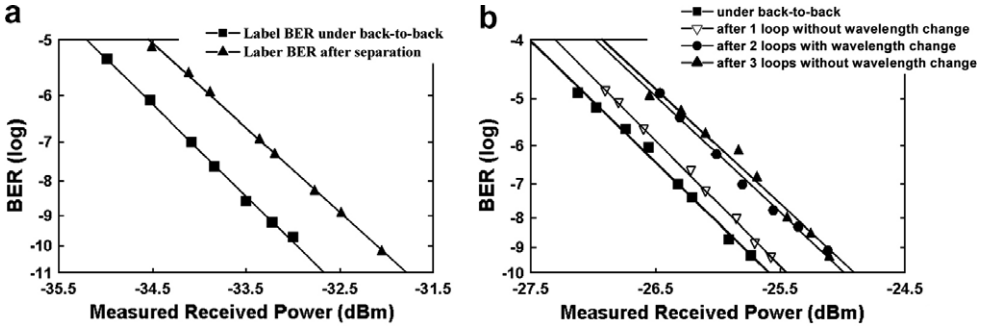

Fig. 5. BER curves of (a) the label in the back-to-back case and after separation from the packet, (b) the payload after various time delays.

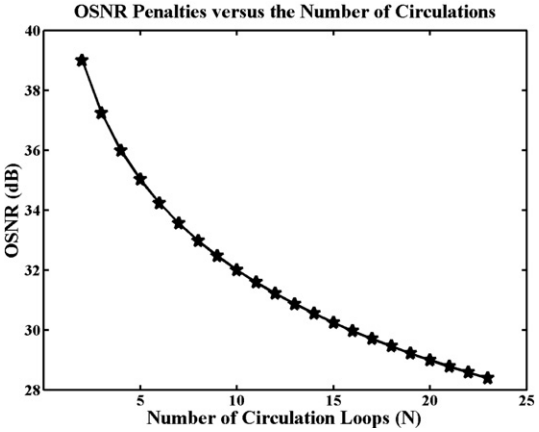

Fig. 6. Ideal curve of OSNR versus Number of circulations, where P_{in} is −11 dBm, noise figure of the EDFA is 6 dB in our experiment.

$$10\lg[L_i(f)] = l_i \sin(2\pi f/f_p + \theta_i) \tag{3}$$

where l_i and f_p are the amplitude and period of the loss ripple, respectively, and θ_i is the phase factor at frequency f with $\theta_i = \pi/2$ at the carrier frequency located at the peak of the LR. Since the LR amplitude of the FBG in our experiment is very small, e.g., ~0.1 dB, we can ignore the high order Fourier series of the transfer function of the LR. Similarly, $G_i(f)$ can be written as:

$$G_i(f) = g_i f_p \cos(2\pi f/f_p + \phi_i) \tag{4}$$

where g_i and f_p are the peak-to-peak amplitude and the period of the GDR, respectively, and ϕ_i is a phase factor showing the offset between the signal frequency and the nearest GDR peak. As discussed in [17], the largest penalty occurs only when the GDR period is close to the bit rate (BR). Thus we calculate the penalty for the worst case where $f_p = BR$. For simplicity we assume that the phase factor of GDR and LR can be expressed as: $\phi_i = \theta_i - \pi/2$ [16,20], which is the case for the FBG used in the experiment. In addition, the high order Fourier expression of the transfer function of the GDR can be ignored, as the g_i in our experiment is small, e.g, ~5 ps. Then we obtain the complete transfer function of $T_i(f)$:

$$\begin{aligned} T_i(f) &= L_i(f) * e^{jG_i(f)} \\ &= e^{\frac{\ln(10)}{10} l_i \sin(2\pi f/f_p+\theta_i)} * e^{j(g_i f_p \cos(2\pi f/f_p+\theta_i-\pi/2))} \\ &= e^{\frac{\ln(10)}{20j} l_i (e^{j(2\pi f/f_p+\theta_i)} - e^{-j(2\pi f/f_p+\theta_i)})} \\ &\quad * e^{j(g_i f_p \cos(2\pi f/f_p+\theta_i-\pi/2))} \end{aligned} \tag{5}$$

In the simulation, for simplicity θ_i is assumed to have no deviation between the signal frequency and the central frequency of the LR and GDR peak for each circulation because the frequency difference after each circulation is equivalent to f_p in our experiment. Using the Jacobi–Anger expansion and Bessel Function generation and keeping the first-order terms for small LR and GDR while neglecting second- and higher-order terms, we obtain:

$$\begin{aligned} T_i(f) &= L_i(f) * e^{jG_i(f)} \\ &= \left(1 + \frac{\ln(10)}{80} l_i e^{j2\pi f/f_p + j(\theta_i - \pi/2)} + \frac{\ln(10)}{80} l_i e^{-j2\pi f/f_p - j(\theta_i - \pi/2)}\right) \\ &\quad * \left(1 + \frac{g_i f_p}{2} e^{j2\pi f/f_p + j\theta_i} + \frac{g_i f_p}{2} e^{-j2\pi f/f_p - j(\theta_i - \pi)}\right) \\ &= 1 + \frac{\ln(10)}{80} l_i e^{j2\pi f/f_p + j(\theta_i - \pi/2)} + \frac{\ln(10)}{80} l_i e^{j2\pi f/f_p - j(\theta_i - \pi/2)} \\ &\quad + \frac{g_i f_p}{2} l_i e^{j2\pi f/f_p + j\theta_i} + \frac{g_i f_p}{2} l_i e^{-j2\pi f/f_p - j(\theta_i - \pi)} \\ &\quad + \frac{\ln(10)}{80} l_i * \frac{g_i f_p}{2} * 2e^{j\pi/2} + \frac{\ln(10)}{80} l_i * \frac{g_i f_p}{2} e^{j4\pi f/f_p + j(2\theta_i - \pi/2)} \\ &\quad + \frac{\ln(10)}{80} l_i * \frac{g_i f_p}{2} e^{-j4\pi f/f_p - j2\theta_i + j\pi} \end{aligned} \tag{6}$$

The last three terms in Eq. (6) are negligible compared to the others. Thus the output signal after i-th circulation can be expressed as:

$$\begin{aligned} b(t) &= \int_{-\infty}^{\infty} A(f) * T_i(f) e^{j2\pi ft} df \\ &= a(t) + \frac{\ln(10) l_i}{80} a(t + 1/f_p) e^{j(\theta_i - \pi/2)} \\ &\quad + \frac{\ln(10) l_i}{80} a(t - 1/f_p) e^{-j(\theta_i - \pi/2)} + \frac{g_i f_p}{2} a(t + 1/f_p) e^{j\theta_i} \\ &\quad + \frac{g_i f_p}{2} a(t - 1/f_p) e^{j(\pi - \theta_i)} \end{aligned} \tag{7}$$

Then the EOP related to the BER in its low regime [21] can be calculated when the phase factor is changed with different number of circulations. Here the EOP can be written as:

$$EOP = \frac{V_{d,1} - V_{d,0}}{V_{u,1} - V_{u,0}}, \tag{8}$$

where V_1 is the voltage level of the minimum "one" rail at the eye center, and V_0 is the voltage level of the maximum "zero" rail. Here the subscript "u" represents the undistorted state of the signal, and the subscript "d" represents the distorted state of the signal.

Numerical results based on Eqs. (7) and (8) show that:

$$\begin{aligned} &P(\theta_i = \pi) < P(\theta_i = 5\pi/4) = P(\theta_i = 7\pi/4) < P(\theta_i = 3\pi/4) \\ &\quad = P(\theta_i = \pi/4) < P(\theta_i = \pi/2) \end{aligned}$$

where $P(\theta)$ denotes the function relating EOP to the phase factor. The transmitted signal after k circulations can be written as:

$$B_k(f) = A(f)^* \prod_{i=1}^{k} T_i(f) \tag{9}$$

where $B_k(f)$ is the spectral expression of the transmitted signal after k circulations, and A(f) is the signal before the optical buffer.

Fig. 7 shows the EOP caused by combined LR and GDR effects when the phase factor is π, with the insets being the eye diagrams of the received signal after N circulations in the buffer. When the phase factor is $\pi/2$, the EOP

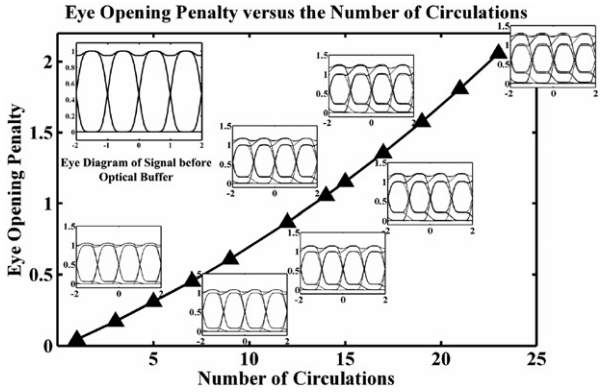

Fig. 7. EOPversus Number of circulations considering effects of grating's LR and GDR together, where l_i is 0.1 dB, g_i is 5 ps, the ripple period $f_p = 1$BR, the phase factor $\theta = \pi/2$.

curve versus the number of circulations (Fig. 8) is different from that in Fig. 7. This is induced by the phase factor change which affects the transfer function in Eq. (5). Fig. 9 compares the EOP results when the phase factor is varied. In Fig. 9, the EOPs with $\theta = \pi/2$ increases faster than the EOPs with other phase factors, because the EOP becomes maximum when $\theta = \pi/2$. We note that the EOP induced by $\theta = \pi/4$ is the same as that induced by

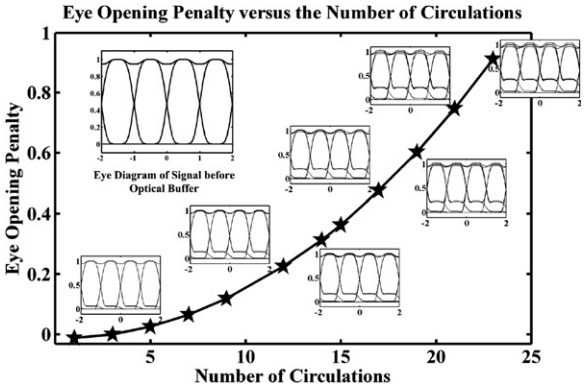

Fig. 8. EOP versus Number of circulations considering effects of grating's LR and GDR together, where l_i is 0.1 dB, g_i is 5 ps, when the phase factor θ is different. the ripple period $f_p = 1$BR, the phase factor $\theta = \pi$.

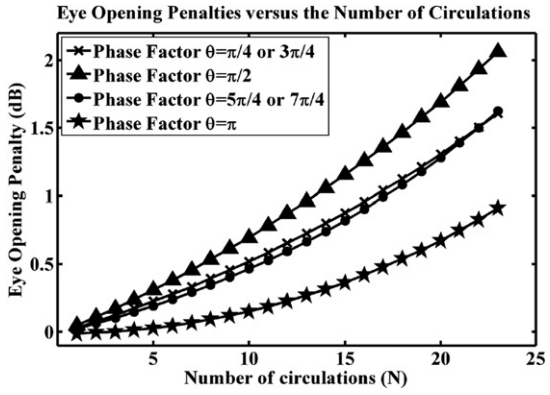

Fig. 9. Comparison of EOP versus number of circulations when the phase factor θ is different.

$\theta = 3\pi/4$, and the EOPs induced by $\theta = 5\pi/4$ and $\theta = 7\pi/4$ are equivalent. The EOP reaches the minimum when the phase factor is π.

According to the analysis, the largest penalty induced by the FBG occurs when $\theta = \pi/2$ [16]. From the results presented, we observe that even small LR and GDR values can degrade the signal quality after ~20 circulations, leading to more than 2 dB power penalty. Besides the LR and GDR of the FBG, the edge slope of the FBG reflection bandwidth may also affect the signal quality. Therefore careful design of the filters to mitigate the signal degradation induced by LR and GDR, and the use of low noise amplifiers are necessary to achieve longer time of storage. With the typical parameters used in the analysis and considering the worst cases, we expect a minimum number of 20 circulations in the loop given a typically required OSNR of 26 dB for a 10 Gb/s receiver.

5. Conclusion

In this paper, we have demonstrated a tunable optical buffer for optical label switching. This optical buffer can achieve tunable and scalable time delays with optional wavelength conversion through proper bias adjustment. In particular, three cases of payload buffering are shown, and BER performance of the proposed optical buffer is evaluated. We also studied three major limiting factors of the optical buffer, including ASE noise accumulation, and the combined LR and GDR effects of the optical filter. Simulation results are provided to show the OSNR degradation, and the EOP induced by the LR and GDR of the FBG, after various number of circulations. We expect a minimum of 20 circulations in such a buffer if typical system parameters are considered. Better performance can be realized by employing low noise figure optical amplifier and minimizing the LR and GDR of the optical filter.

Acknowledgements

The authors acknowledge the support from the National Natural Science Foundation of China under the grants 60407008, the 863 High-Tech program (2006AA01Z255), the key project of Ministry of Education under the grant 106071, and the Fok Ying Dong Fund under the grant101067. The authors also thank Fangfei Liu for helpful discussions.

References

[1] D.J. Blumenthal, B.-E. Olsson, G. Rossi, et al., J.Lightwave Technol. 18 (2000) 2058.
[2] Y.K. Lize, X. Liu, R. Kashyap, IEEE Photon. Technol. 18 (2006) 1140.
[3] X. Ma, Opt. Commun. 269 (2007) 53.
[4] W.D. Zhong, R.S. Tucker, J.Lightwave Technol. 19 (2001) 1085.
[5] A. Shacham, B.A. Small, K. Bergman, ECOC2006, paper We3 (2006).

[6] R.S. Tucker, P.C. Ku, C.J. Chang-Hasnain, J. Lightwave Technol. 23 (2005) 4046.
[7] C.J. Chang-Hasnain, P.C. Ku, R.S. Tucker, in: Proceedings of Optical Fiber Communication (OFC), Paper JWA33 (2005).
[8] Y.K. Yeo, J. Yu, G.K. Chang, J. Lightwave Technol. 24 (2006) 365.
[9] A. Chowdhury, Y.K. Yeo, J. Yu, G.K. Chang, IEEE Photon. Technol. Lett. 18 (2006) 1176.
[10] T. Kawanishi, S. Oikawa, K. Higuma, M. Izutsu, IEEE Photon. Technol. Lett. 14 (2002) 1454.
[11] T. Kavanishi, M. Izutsu, IEICE Trans. Electron., E86-C 7 (2003) 1230.
[12] H.J. Lee, S.J.B. Yoo, V.K. Tsui, S.K.H. Fong, IEEE Photon. Technol. Lett. 13 (2001) 635.
[13] M. Jeon, Z. Pan, J. Cao, S. Yoo, Proc. Optical Fiber Communication (OFC), Paper TuQ4 (2003).
[14] M. Izutsu, S. Shikama, T. Sueta, IEEE J. Quantum Electron. 17 (1981) 2225.
[15] Y. Yamada, K. Sasayama, K. Habara, Proc. Optical Fiber Communication (OFC), Paper WD2 (96).
[16] X. Liu, X. Wei, A.H. Gnauck, et al., IEEE Photon. Technol. Lett. 17 (2005) 82.
[17] X. Liu, L.F. Mollenauer, X. Wei, IEEE Photon. Technol. Lett. 16 (2004) 305.
[18] G.P. Agrawal, in: Optical Fiber Communication Systems, Wiley, New York, 2002, p. 261.
[19] J. Kissing, T. Gravemann, E. Voges, IEEE Photon. Technol. Lett. 15 (2003) 611.
[20] T. Niemi, M. Uusima, H. Ludvigsen, IEEE Photon. Technol. Lett. 13 (2001) 1334.
[21] J.D. Downie, J. Lightwave Technol. 23 (2005) 2031.